Theory of an electro-cordic field operating in quantum systems. II

R. Wayte.

29 Audley Way, Ascot, Berkshire, SL5 8EE, England, UK

E-mail: rwayte@googlemail.com

Research article. Submitted to vixra.org 22 August 2012

Abstract: The physical nature of proposed electro-cordic guidewaves has been demonstrated by applying the theory to relativistic potential wells and a simple harmonic system. Interference observed in Young's slits and the Michelson interferometer has also been explained as due to active guidewave fields controlling photons. Entanglement is interpreted in terms of real coupling by interlinked guidewaves between particles or photons; so wavefunction collapse occurs when this physical link is broken. Superconductivity requires real material binding for electron-pair creation and correlation.

Keywords: quantum mechanics

PACS Codes: 03.65.-w, 03.65.Ta

1 Introduction

In the companion paper (Wayte, 2012, Paper I) the need for a causal quantum theory to explain experimental results properly was seen as a natural continuation of classical physics from astronomical bodies to sub-atomic particles. Then the proposed electro-cordic guidewaves were generated by particles to convey interactions at the velocity of light or faster. Application of this theory to the hydrogen atom showed the direct transfer of concepts like orbits from astronomy and general relativity theory to atoms and quantum theory. Remarkable compatibility was found between the relativistic systems.

Here, the aim in Section 2 is to reveal the physical nature of electro-cordic guidewaves of de Broglie wavelength described by the wavefunction, in systems such as a potential well and simple harmonic oscillator. Section 3 covers detailed guidewave explanations for interference phenomena seen in Young's slits and Michelson interferometer experiments. Entanglement is interpreted in Section 4 as a real superluminal guidewave link between particles or photons, which breaks during wavefunction collapse. In Section 5 the reality of guidewave trajectories between charges is demonstrated. Finally, Section 6 describes the material binding of electron-pairs in superconductivity, which leads to a heuristic explanation for high temperature superconductors.

Overall, the guidewave interpretation of the wavefunction is first and necessary, while the probability interpretation is not always appropriate. Standard quantum theory only describes results of experiments, without interpretation involving mechanisms such as guidewaves and wavefunction collapse, or internal structures of particles and photons.

2 Applications of a relativistic wave equation

Three of the standard applications of Schrödinger's non-relativistic equation will now be considered from a relativistic viewpoint, in order to emphasise the role of the de Broglie wavelength and necessity of guidewave physical reality. The non-relativistic equation is mathematically easier to apply, but it is incomplete.

2.1 The infinite square well potential

This is usually given as the simplest example of a theoretical non-relativistic wave mechanical system. It can be converted to a relativistic system to confirm the existence of guidewaves with de Broglie wavelength. From Schiff (1968) p38, the time-independent Schrödinger non-relativistic wave equation, corresponding to the particle equation $\left(p^2/2m + V(x) = E\right)$, is:

$$-\frac{\hbar^2}{2m}\frac{d^2u}{dx^2} + V(x)u = Eu \ , \qquad (2.1)$$

where V(x) is zero within the well defined by ($-a < x < +a$), but is infinite outside. For the usual interpretation, the ground state eigenfunction is then:

$$u_1 = a^{-1/2}\cos\left(\frac{\pi x}{2a}\right) = a^{-1/2}\cos\left[\left(\frac{2mE_1}{\hbar^2}\right)^{1/2} x\right] = a^{-1/2}\cos\left(\frac{p_1}{\hbar}x\right) \ , \qquad (2.2)$$

with energy eigenvalue $(E_1 = \pi^2\hbar^2/8ma^2)$. Given that the de Broglie wavelength is defined as $(\lambda_B = h/p)$, then we have $(\lambda_{B1} = 4a)$. This fit of $(\lambda_{B1}/2)$ into the well width is the essential physical connection between the well and the guidewave, analogous to a standing sound wave in an organ pipe. The guidewave emitted by the particle in the forward direction of travel can then reflect from both walls before returning to the particle *from the rear*, in phase 2π later. Single value wave amplitude at the source particle is thereby achieved by constructive interference between the source and reflected guidewaves.

For the travelling guidewave interpretation of Eq.(2.1), the amplitude ground state solution is:

$$u_1 = a^{-1/2}\cos\left(\frac{\pi x}{2a} + \phi\right) \ , \qquad (2.3a)$$

with the same energy eigenvalue E_1. Phase ϕ is determined by the instantaneous particle position. For example, if the particle moves with velocity v from ($x = 0$) at ($t = 0$) towards the barrier at ($x = +a$), then the instantaneous guidewave amplitude at position x and time t is:

$$u_1 = a^{-1/2}\cos\left(\frac{x}{a}\frac{\pi}{2} - \frac{vt}{a}\frac{\pi}{2}\right) \ . \qquad (2.3b)$$

Therefore, from the start at (t = 0), the amplitude u_1 at the barrier position (x = a) increases sinusoidally from zero up to $+a^{-1/2}$, then decreases through zero down to $-a^{-1/2}$, and then increases back to zero after total time (t = 4a/v). The particle has moved at constant velocity v from (x = 0) to (x = +a) where it was reflected towards (x = –a) to be reflected again back to (x = 0). There is no concentration of the particle around (x = 0). The guidewaves are reflected continuously at the barriers and confined within the well throughout.

For the standard interpretation of quantum theory, equation (2.2) represents probability amplitude. This is arbitrary but may be justified when interactions between systems are considered because the particle would on average appear to be around (x = 0). However, it is important to remember that the analysis leading to eigenfunction Eq.(2.2) depends on the particle traversing the box back and forth at constant velocity (v = p/m), for $E_1 = p_1^2/2m$. It cannot really avoid the walls to concentrate at the centre because that would make p vary and invalidate the initial conditions, so the theory would no longer be self-consistent. Nevertheless, the amplitude Eq.(2.2) can be taken as representing a standing guidewave to locate the particle on average, as far as interactions with other particles are concerned.

This analysis will now be carried over to the relativistic wave equation as follows. The relativistic particle equation $(E^2/c^2 = p^2 + m_o{}^2c^2)$ has an equivalent Schrödinger wave equation inside the potential well:

$$\left(\frac{E}{c}\right)^2 u = \left(-\hbar^2 \frac{d^2}{dx^2} + m_o{}^2c^2\right)u \,. \qquad (2.4)$$

The ground state eigenfunction for the probability interpretation is:

$$u_1 = a^{-1/2}\cos\left(\frac{\pi x}{2a}\right) = a^{-1/2}\cos\left[\left(\frac{E_1{}^2/c^2 - m_o{}^2c^2}{\hbar^2}\right)^{1/2} x\right] = a^{-1/2}\cos\left(\frac{p_1}{\hbar}x\right) \,. \quad (2.5)$$

Given ($p_1 = h/\lambda_{B1}$), then again ($\lambda_{B1} = 4a$), which proves that the relativistic de Broglie wavelength $[\lambda_B = h(1 - v^2/c^2)^{1/2}/m_o v]$ matches the well dimensions for resonance. Thus, it is the physical nature of real guidewaves which essentially determine the allowed energies of particles in wells. The energy eigenfunction is dependent upon the momentum by means of λ_B governing the fit to the well width.

Energy eigenvalues above the ground state may be derived in the usually way, allowing for ($n\lambda_B$ = 4a). Each increase in energy corresponds with an extra half de Broglie wavelength being fitted into the potential well full width. This is obviously analogous to standing waves in organ pipes and supports the reality of guidewaves.

For Eq.(2.5), the complete time-dependent wavefunction is:

$$\psi_1(x,t) = u_1(x)\exp(\pm i E_1 t/\hbar) \quad , \tag{2.6}$$

where E_1 is the particle *relativistic* energy. It is this circularly polarised guidewave which propagates at the velocity of light and interacts with other particles, or itself by reflection within a system to generate the de Broglie wavelength by interference. Therefore Eqs.(2.2), (2.3) and (2.5) only represent the *peak amplitude* of the guidewave's high frequency oscillation, as it varies from place to place within the well.

2.2 Finite square-well potential

This example has always been used to explain quantum mechanical tunnelling as a particle statistical phenomenon. Again, Schrödinger's non-relativistic equation (2.1) can be applied for the case within the well, where [V(x) = 0] for (–a < x < a), and outside where [V(x) = V_o > E] for (|x| > a). From Schiff (1968) p40, these two regions yield the general wavefunction solutions, respectively:

$$u(x) = A\sin\alpha x + B\cos\alpha x, \qquad \alpha = +\left(\frac{2mE}{\hbar^2}\right)^{1/2} = \frac{p}{\hbar} \quad , \tag{2.7a}$$

$$u(x) = C\exp-\beta x + D\exp+\beta x, \qquad \beta = +\left(\frac{2m(V_o - E)}{\hbar^2}\right)^{1/2} = \frac{p'}{\hbar} . \tag{2.7b}$$

For continuous u and du/dx at (x = ±a), the energy eigenvalues are found by solving numerically the equations:

$$[\alpha\tan\alpha a = \beta] \quad \text{or} \quad [\alpha\cot\alpha a = -\beta], \quad \text{and} \quad [\alpha^2a^2 + \beta^2a^2 = 2ma^2V_o/\hbar^2] \, . \tag{2.7c}$$

It is interesting to calculate a simple ground state example such as when ($\alpha = \beta = \pi/4a$) with ($E_1 = V_o/2$), which occurs when ($V_o = \pi^2\hbar^2/16ma^2$); see Figure 1, where:

$$u(x) \underset{(-a\le x\le a)}{=} B_1\cos\left(\frac{\pi}{4}\frac{x}{a}\right), \quad \text{and} \quad u(x) \underset{(|x|\ge a)}{=} C_1\exp\left(-\frac{\pi}{4}\frac{x}{a}\right) \quad . \tag{2.8a}$$

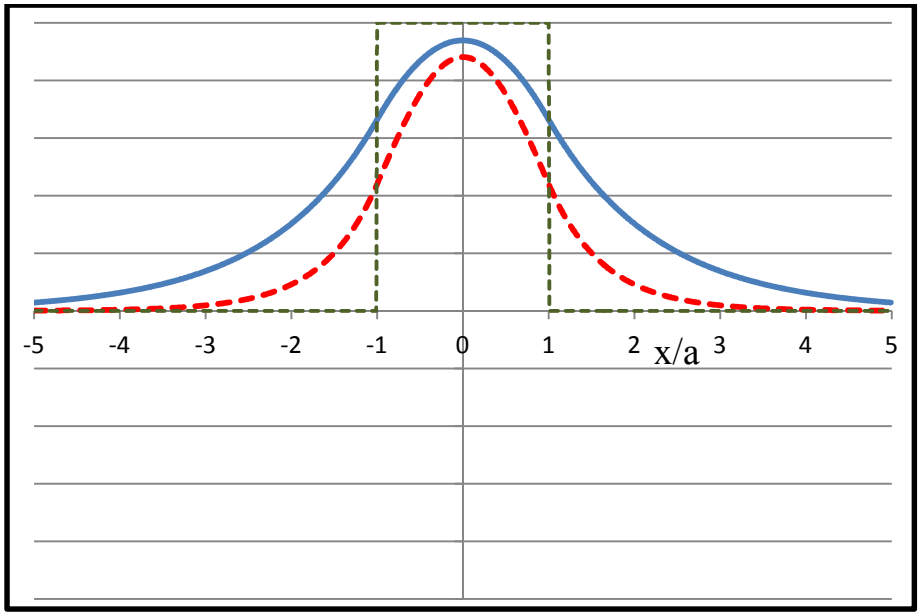

Fig.1 Ground state wavefunction amplitude Eq.(2.8a) (—), and probability density $u(x)^2$ (- - -). The classical position density is also shown (▪▪▪▪).

Then from Eq.(2.7a):

$$p_1 = (2mE_1)^{1/2} = (\hbar\pi/4a) \quad , \tag{2.8b}$$

so that the de Broglie wavelength is:

$$\lambda_{B1} = h/p_1 = 8a \quad . \tag{2.8c}$$

This λ_{B1} is double the previous value (where $V_o = \infty$), with momentum 2 times less and energy 4 times less. So, the guidewaves penetrate the wall around distance 'a' on average, before being reflected back into the well. This is followed by reflection again at the other wall, before returning to the source particle from the rear in the required phase 2π for single valued amplitude.

There is a simple general relationship between E_1 and an arbitrary value of V_o :

$$\frac{E_1}{V_o} = \cos^2\left(\frac{2\pi a}{\lambda_{B1}}\right) \quad , \tag{2.8d}$$

which confirms through Eqs.(2.8b),(2.8c) that guidewavelength λ_{B1} is determined by the real well dimensions.

Figure 2 shows the wavefunction for a particle with 3 times the momentum within a wider well, for ($\alpha = \beta = 3\pi/4a$). That is:

$$u(x)_{(-a \le x \le a)} = B_3 \cos(3\frac{\pi}{4}\frac{x}{a}), \quad \text{and} \quad u(x)_{(|x| \ge a)} = C_3 \exp(-3\frac{\pi}{4}\frac{x}{a}). \qquad (2.8e)$$

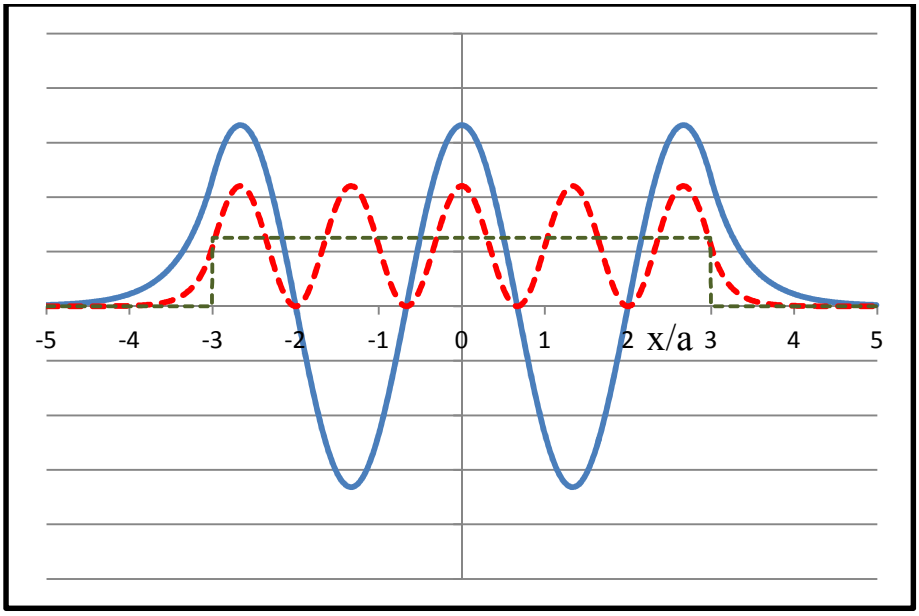

Fig.2 Third harmonic wavefunction amplitude Eq.(2.8e) (—), and probability density $u(x)^2$ (- - -). The classical position density is also shown (▪▪▪▪).

Now, for the equivalent relativistic analysis, the wave equation produces solutions:

$$u(x) = A\sin\alpha x + B\cos\alpha x, \qquad \alpha = +\left(\frac{E^2/c^2 - m_o{}^2c^2}{\hbar^2}\right)^{1/2} = \frac{p}{\hbar}, \qquad (2.9a)$$

$$u(x) = C\exp-\beta x + D\exp+\beta x, \qquad \beta = +\left(\frac{(V_o - E)^2/c^2 - m_o{}^2c^2}{\hbar^2}\right)^{1/2}. \qquad (2.9b)$$

The energy eigenvalues are found by eliminating E from these equations, then specifying V_o and solving numerically with the use of:

$$[\alpha \tan \alpha a = \beta] \quad \text{or} \quad [\alpha \cot \alpha a = -\beta]. \qquad (2.10)$$

Again we can calculate a simple ground state example such as when ($\alpha = \beta = \pi/4a$) with ($E_1 = V_o/2$). Then:

$$p_1 = (E_1{}^2/c^2 - m_o{}^2c^2)^{1/2} = \hbar(\pi/4a), \qquad (2.11a)$$

so that the de Broglie wavelength is the same as for the non-relativistic case:

$$\lambda_{B1} = h / p_1 = 8a \quad , \tag{2.11b}$$

which confirms that the relativistic de Broglie wavelength matches the well dimensions, as governed by the resonance of real guidewaves.

When interpreting the guidewave intensity $|\psi(x)|^2$ as a probability density, the probability of a particle tunnelling through the wall may be calculated. What this means physically is that the wall of potential V_o is not impervious in a classical sense. It consists of repelling charges between which the particle may squeeze due to local fluctuations in the quantised electric field. Penetrating particles which do not get through the wall completely are reflected back into the well. Evanescent waves in optics demonstrate quantum mechanical tunnelling by photons.

It is not always necessary for the wavefunction to represent probability density in addition to the guidewave amplitude. For example, the hydrogen radial and angular eigenfunctions have to be selected from a number of mathematical solutions. Consequently, the probability density interpretation is thought to apply only to guidewaves emitted in the direction of motion. Guidewaves emitted laterally do not cause the particle to zigzag either side of its classical trajectory, as suggested by Bohm & Hiley (1993). We saw in the companion paper how the hydrogen radial eigenfunction represents possible guidewave amplitude, not electron position probability. The electron travelled in precise controlled orbits, compatible with sharp energy spectra.

2.3 Linear harmonic oscillator

Some features of the harmonic oscillator will be described which demonstrate the physical properties of the wavefunction. Classically, the energy equation is:

$$\frac{p^2}{2m} + \frac{1}{2}Kx^2 = E \quad , \tag{2.12a}$$

where the restoring force on the particle is ($F = -Kx$) and the potential energy is ($\frac{1}{2}Kx^2$) increasing from zero at ($x = 0$) to a maximum ($E = \frac{1}{2}Kx_{max}^2$).

In quantum theory, Schrodinger's non-relativistic wave equation is given by Schiff p67 as:

$$-\frac{\hbar^2}{2m}\frac{d^2u}{dx^2} + \frac{1}{2}Kx^2u = Eu \, , \tag{2.12b}$$

The general wavefunction solution of this is conveniently expressed:

$$u_n(\xi) = N_n H_n(\xi) \exp(-\tfrac{1}{2}\xi^2) \quad , \tag{2.13}$$

for $(\xi = \alpha x)$; $\alpha = (\frac{mK}{\hbar^2})^{1/4}$; $N_n = (\frac{\alpha}{\pi^{1/2} 2^n n!})^{1/2}$; $H_n = (-1)^n \exp(\xi^2) \frac{\partial^n}{\partial \xi^n} \exp(-\xi^2)$.

The energy eigenvalues are derived in Schiff p69 as:

$$E_n = (n + \tfrac{1}{2})\,\hbar \left(\frac{K}{m}\right)^{1/2} \quad . \tag{2.14}$$

When (n = 0), the ground state solution is as shown in Figure 3:

$$u_o(\xi) = \left(\frac{\alpha}{\pi^{1/2}}\right)^{1/2} (1)\ \exp(-\tfrac{1}{2}\xi^2) \quad . \tag{2.15}$$

The guidewave intensity equivalent to probability density $|u(\xi)|^2$ is also shown; and the *classical* position density proportional to $(\xi_o^2 - \xi^2)^{-1/2}$, for $(\xi_o = 1)$. The wavefunction represents guidewave amplitude as a function of x, at the instant when the particle is at position (x = 0). Likewise, Figure 4 shows the wavefunction for harmonic (n = 4) as:

$$u_4(\xi) = \left(\frac{\alpha}{\pi^{1/2} 16 \times 24}\right)^{1/2} \left(16\xi^4 - 48\xi^2 + 12\right) \exp(-\tfrac{1}{2}\xi^2) \quad . \tag{2.16}$$

The guidewave intensity equivalent to probability density $|u_4(\xi)|^2$ is shown; and the *classical* position density proportional to $(\xi_o^2 - \xi^2)^{-1/2}$, for $(\xi_o = 3)$.

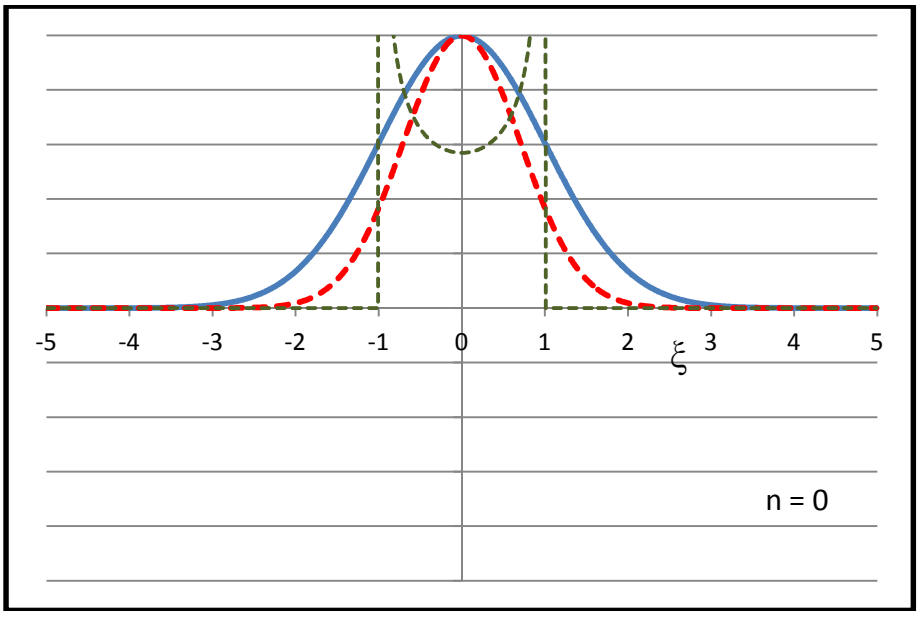

Fig.3 Ground state wavefunction amplitude Eq.(2.14) (—), and probability density $u_o(\xi)^2$ (- - -). The classical position density is also shown (▪▪▪▪).

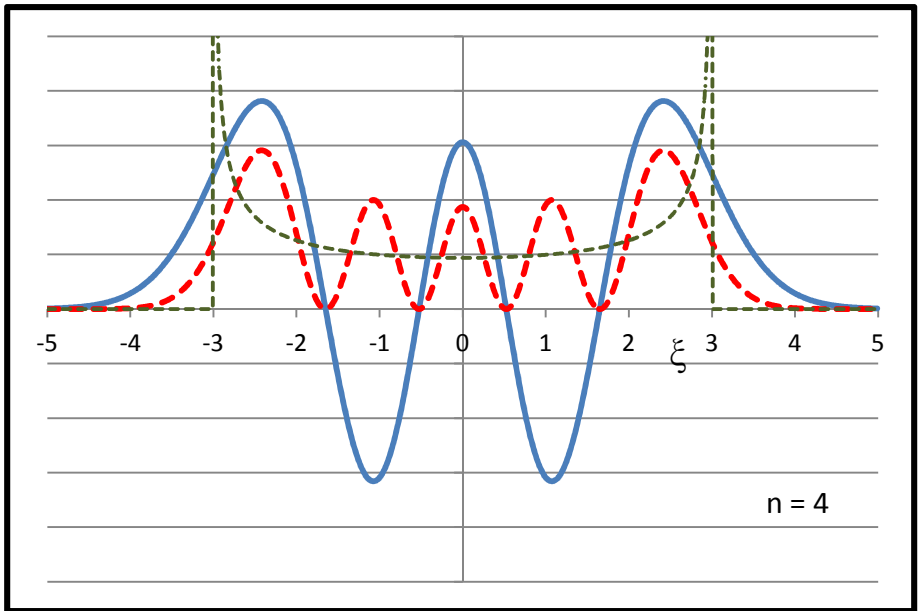

Fig.4 The harmonic wavefunction amplitude Eq.(2.15) (—), and probability density $u(\xi)^2$ (- - -). Classical position density is shown (▪▪▪▪).

It is immediately apparent that Figure 3 is very similar to Figure 1 because an oscillating particle restrained by a central force behaves somewhat like a free particle constrained by low potential walls. Similarly, Figure 4 is like Figure 2 where the wavefunction/guidewaves accommodate the particle constraints, and thereby determine the allowed energy levels.

We can interpret the ground state wavefunction Eq.(2.15) in terms of the de Broglie wavelength, to illustrate its control, as was shown in Eqs.(2.7a) and (2.8c):

$$u_o(\xi) = \left(\frac{p_{max}}{\hbar\pi^{1/2}}\right)^{1/2} \exp -\frac{1}{2}\left(\frac{p_{max}}{\hbar}x\right)^2 = \left(\frac{1}{x_{max}\pi^{1/2}}\right)^{1/2} \exp -\frac{1}{2}\left(\frac{x}{x_{max}}\right)^2, \qquad (2.17)$$

where p_{max} is the maximum momentum found at (x = 0) in Eq.(2.12a). This means that the *minimum* de Broglie wavelength ($\lambda_{B0min} = h/p_{max} = 2\pi x_{max}$) is the standard for determining the energy eigenvalues in the linear harmonic oscillator. For energy states in general, the minimum de Broglie wavelength would be ($\lambda_{BNmin} = h/p_{max} = 2\pi x_{max}/N$), where N = 1, 3, 5, - - -).

In reality, the value for λ_{B0min} is slightly smaller, but it is still determined by x_{max}. That is, the relativistic equivalent of Eq.(2.12a) is:

$$p^2c^2 = (E - \tfrac{1}{2}Kx^2)^2 - m^2c^4 \ , \qquad (2.18)$$

so for (x = 0), and (p = 0) respectively, we find:

$$[p_{max}{}^2c^2 = E^2 - m^2c^4] \ , \quad \text{and} \quad [0 = (E - \tfrac{1}{2}Kx_{max}{}^2)^2 - m^2c^4] \ . \qquad (2.19)$$

Then, upon eliminating E :

$$[p_{max}{}^2 = mKx_{max}{}^2 + (K^2x_{max}{}^4)/4c^2] \ , \text{and} \quad [\lambda_{B0\,min} = h/p_{max}] . \qquad (2.20)$$

To summarise this Section, the wavefunction for a particle, restrained by a square well potential or linear oscillator, has been interpreted as the amplitude of the real guidewaves emitted spontaneously and continuously by the particle itself. The square of the wavefunction is then guidewave intensity, which may be equivalent to probability density in some circumstances but not necessarily always. Obviously, this ontological interpretation of the wavefunction has been compatible with the particle's reality.

3. Interference phenomena

In physical optics, interference profiles have always been explained accurately as a wave phenomenon; see Jenkins and White (1957). For example, Young's slits eventually produce fringes on a screen even when the light source is very weak. Similarly, the two-arm Michelson interferometer directs individual photons proportionally, in the same way as calculated for a bright light flux. The wave and particle nature of light are therefore compatible in a single experiment, and the concept of continuous photon trajectories is advantageous. However, problems of *interpretation* arise when a predictable high quality interference pattern with its information content grows from nothing as single photons pass through the system. Standard quantum theory simply states what will probably be observed and is apparently incapable of addressing the need for physical processes underlying such observational results.

One viable explanation requires every photon to interfere with its own advance guidewave field, which is sent ahead of it at superluminal velocity to prepare the system by *interacting* with the Coulomb fields of nearby atoms. Similarly, when interference of electron beams occurs, each electron interferes with its own guidewave field, and fringe profiles are determined by the de Broglie wavelength according to wave theory; see Jönsson (1974), Hitachi (2012).

Some examples of interference, which benefit from an explanation involving guidewaves, will now be given.

3.1 Young's slits

We have suggested that the quanta and particles passing through Young's slits emit guidewave fields which help guide them individually to fringes, being distributed according to the predicted wave amplitude while arriving randomly in time. A guidewave induces the local environment of the slits' to impose necessary angles of trajectory by incorporating the distance to the screen and induced excitation of the screen atoms.

Some understanding of fringe patterns may be derived by relating to the electromagnetic theory of radiation from antennas. Consider first the diffraction pattern of a single slit illuminated by a coherent beam of light, see Jenkins and White (1957) p.291. The slit is regarded as being equivalent to Huygen elemental isotropic radiators which generate interference in amplitude at any given point on the screen. Such a diffraction pattern is analogous to the radiation polar diagram of Hertzian dipoles stacked across the slit; see Glazier and Lamont (1958), Terman (1955). In such dipoles, the energy is introduced continuously as a sinusoidal current but is converted into coherent radiation quanta by the oscillating electrons. These quanta are emitted at random but the average rate of emission, at a given angle from a dipole, is governed by electric potential and continuous field produced by many charges within the dipole. This controlled randomness, with strict dependence upon net Coulomb field strength in a given direction, is fundamental. It appears that the electrons take energy steadily from the input source as they are being accelerated, and then shed energetic quanta from their fields. The coherence of radiated quanta indicates continuous interaction due to guidewaves linking all quanta as they are created.

If two antennas are placed side by side and energised in phase, then a receiver will detect interference which depends upon its position in the crossed radiation field. Participation of the receiver is essential for interference to occur because without it the two beams of radiation would carry on into space without interfering.

Now, the photons excite electrons in the slit jaws into oscillation, analogous to a receiving antenna in which electrons are excited by incoming radiation and may re-radiate directionally. An optical slit behaves much like a slot antenna. These slit electrons then react back through their Coulomb fields on the photons, and scatter them. However, the

screen is also involved in forming a Fraunhofer diffraction pattern so each photon has its own guidewaves travelling ahead of it to establish the screen field and then the overall slit field in order to set the *angular* trajectory of the photon from the slit. Involvement of the complete apparatus is natural since transmitter and receiver antenna polar diagrams will include nearby reflector elements.

It is helpful to reconsider real properties of interference patterns, in order to eliminate non-viable fantastic explanations. Figure 5 shows how Young's double slit produces a far-field interference pattern on a screen in the usual manner from wave theory. That is:

$$x = m\lambda\left(\frac{D}{d}\right), \quad \text{for} \quad m = 0, 1, 2, 3, \cdots . \quad \text{BRIGHT FRINGES} \qquad (3.1)$$

or

$$x = \left(m + \tfrac{1}{2}\right)\lambda\left(\frac{D}{d}\right) \quad . \qquad \text{DARK FRINGES} \qquad (3.2)$$

The fringe intensity profile is given by :

$$I = I_o \cos^2\left(\frac{2\pi}{\lambda}\left(\frac{d}{D}\right)\frac{x}{2}\right) \quad . \qquad (3.3)$$

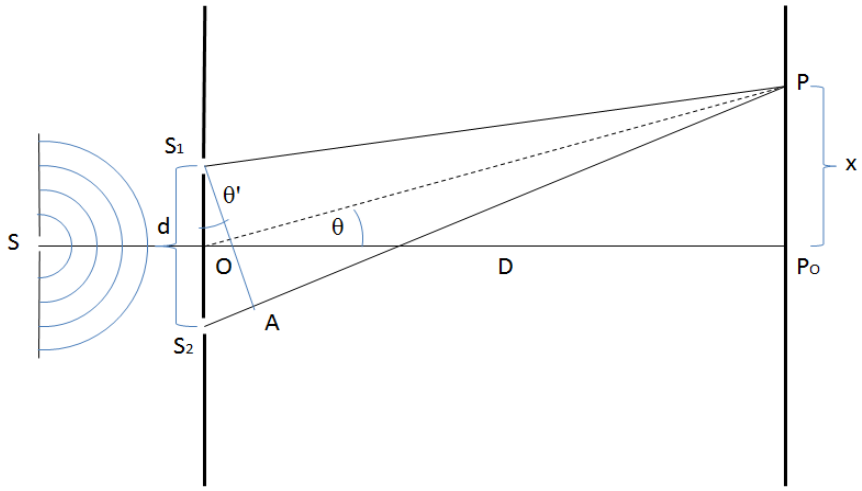

Figure 5 Young's double-slit experiment produces an interference pattern on a screen.

This is the observed profile, which is unlike that predicted by Bohm's theory wherein photons cannot cross the axis and fringe profiles are different. Herein, I_o is double the intensity of the uniform illumination that would occur if there were no interference; so photons are being moved from potential dark fringe positions to neighbouring bright fringes. When D is varied, bright fringes are located along lines of constant θ. This angle is established *near the slits in advance* of photons travelling distance D to their

destination at P (say 20 nsec for D = 6m). If the photon is absorbed by the screen or detector, its total energy including gathered guidewave energy is converted to kinetic energy or heat. This means that wavefunction collapse is total. A new guidewave/wavefunction will be generated by an excited electron. If the guidewave and photon are reflected by the screen, they will have a phase shift of π.

Various animations of interference on the Internet convey the optical illusion that power flows from the origin O, but of course power flows from the slits. This means that photons heading straight for the bright fringes are unperturbed as they cross regions where dark fringes *would be observed if* the screen were moved there. When the screen is moved inward say, the photon trajectories for bright fringes shift laterally due to momentum being induced by the guidewave field at the slit, in accord with the current screen position.

For interference generation at all, there must be feedback of the guidewave through the other slit in order to make the amplitude *at the photon* coherent and single valued. The photon interferes with its own reflected guidewave, subject to participation of the excited slits and screen Coulombic fields. The interference pattern is naturally set-up by a photon's guidewaves obeying wave theory in advance, so every photon is guided continuously and smoothly from the source to the screen. However, it is interesting to estimate roughly how much lateral momentum would be necessary to produce an interference pattern from a uniform field, by quantum jumps. First, let there be *theoretically* uniform illumination on the screen, then to build a bright fringe, it is necessary for some photons (32%) to jump from a dark position to the bright position. If these photons have forward momentum ($p = h\nu/c$), and each acquires lateral momentum p_x to move half a fringe, then:

$$\frac{p_x}{p} \approx \Delta\theta = \frac{\Delta x}{D} = \frac{\lambda/2}{d}, \qquad (\Delta m = \tfrac{1}{2}) \quad , \tag{3.4}$$

and so,

$$p_x = \frac{h}{2d} \quad . \tag{3.5}$$

Here, the slits appear to interact with each other and the screen and source S, by way of guidewaves.

Some tests can be carried out on the interference pattern:

Test 1, Figure 6: An aperture stop A, mid-field stop M, and screen field stop F may be introduced to confirm that photons travel in straight lines without wild zigzagging, and half of them do cross the centre-line (unlike in Bohm's theory). Any zigzagging would ruin the phase coherence necessary for interference.

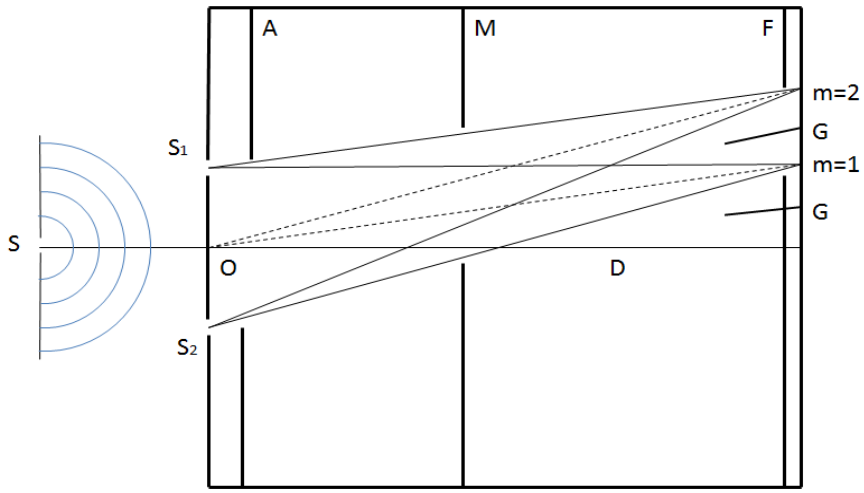

Figure 6 Aperture stops A, M, F, confirm straight-line photon trajectories and independence of nearby fringes

Test 2: The screen stop F or the screen itself may be reduced to a single fringe width to prove that adjacent fringes do not contribute to each other. Similarly, stops G may be put between bright fringes without affecting them. Therefore, a fringe pattern does not involve the entire apparatus, except for minor edge effects.

Test 3, Figure 7: An inclined laser beam with its directional polar diagram may illuminate one slit more than the other. On the screen, the depth of interference will be reduced and will sit upon a continuum of light. If the light intensity is decreased to ensure that only a single photon is in the system at a time, then each photon must either interfere with itself, or not interfere at all. This can only be achieved if the laser polar diagram is involved in determining the interference pattern. Therefore, photon guidewaves must refer to source S

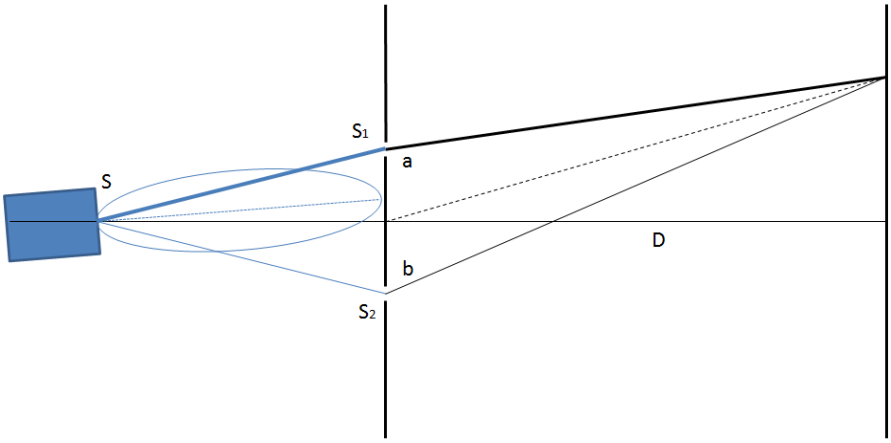

Figure 7 An inclined laser beam may illuminate the slits unequally

and be subject to the polar diagram weighting as well as path length considerations. The fringe intensity is given by:

$$I_{ab} = a^2 + b^2 + 2ab\cos\left(\frac{2\pi x}{\lambda}\left(\frac{d}{D}\right)\right) \quad , \qquad (3.6)$$

where *a* and *b* are the effective amplitudes at S_1 and S_2 respectively.

Test 4, Figure 8: An off-axis coherent laser beam illuminates a double slit and screen. The central bright fringe is at P_0' on the laser axis with the fringe pattern determined by the angle α from this, in the usual manner calculated from wave theory. The photons therefore retain some of their pre-slit forward momentum and polar diagram; travelling in straight lines and crossing the axis as required. In addition, the phase of slit S_2 relative to slit S_1 depends upon arbitrary choice of ϕ, so a photon and its guidewave need to refer to the source S throughout its existence, as well as to the slits and screen.

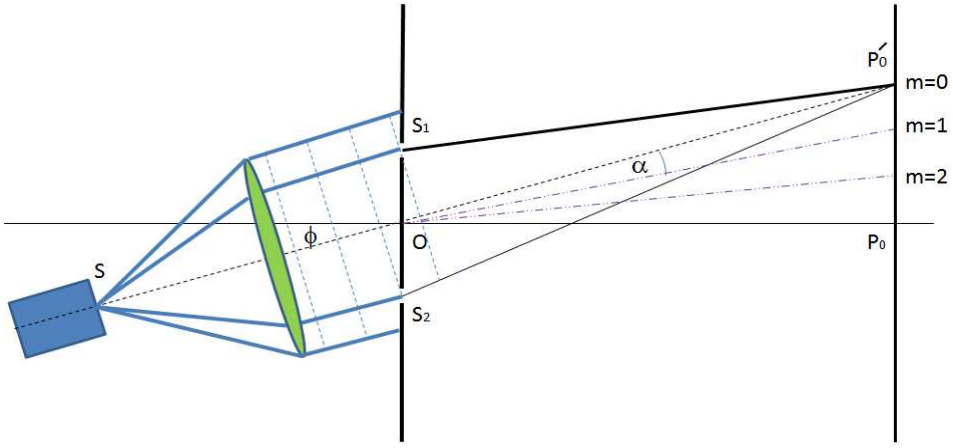

Figure 8 An off-axis laser beam illuminates the slits with different phases

In another experiment (Fonseca et al. 1999), the quantum interference by a non-local double slit strongly indicates that guidewaves lead the way through the system in addition to coupling the entangled photons. An earlier experiment (Pfleegor & Mandel, 1967) involving interference produced by two *separate* lasers emitting single photons is interpretable by letting a photon's guidewaves assess the complete system dimensions of the two lasers plus screen in order to select its ultimate fringe position.

For a double- or multi-slit experiment it is necessary that every incident photon assesses the geometry by sending guidewaves through all slits ahead of it, as already allowed by quantum theory, although the photon really does pass through only one slit. Every photon therefore interacts with its own guidewave field, and the electromagnetic field of the slit atoms and detector/screen.

Finally, when a parallel beam of mono-energetic *particles* falls upon slits, it is the de Broglie guidewavelength which interacts with the slit jaws to cause scattering, and the guidewave interference governs particle trajectories in great detail. Given that the generation of a de Broglie wavelength depends upon self interference of the fundamental guidewave, it is necessary that the guidewaves pass through one slit and reflect from the screen before returning through the other slit, in order to assess the whole system continuously, before and after the particle passes through *one* slit and is guided to its place on the screen. In reality, a flow of single electrons through the system will steadily build an interference pattern from nothing; see Jönsson (1974), Hitachi (2008).

Recent measurements of atomic interference have shown how atomic microwave absorption is enough to eliminate any interference pattern, see (Durr, Nonn & Rempe, 1998). This is in agreement with Bohm's postulate that heat destroys quantum entanglement, as demonstrated for Cooper-pairing in superconductivity. Other experiments on neutron interference have clearly revealed how it is necessary for a neutron to interfere with its own field; see review by Selleri (1982) p.1099.

According to Bohm & Hiley (1993), particles pass through the slits in *laminar* flow then diverge and bunch into unusual fringe profiles while never crossing the plane of symmetry. This contrasts with our more standard interference model, as calculated from wave theory, wherein particles or photons are allowed to scatter and cross trajectories from every element of each slit to produce the *observed* fringe profiles.

3.2 Michelson Interferometer

This two-beam instrument is well understood from wave theory in terms of division of amplitude; see Jenkins & White (1957) p.244. However, there are problems of interpretation because individual photons are not thought to divide into two less energetic photons at the beamsplitter; and other evidence indicates that each photon must interfere with itself to determine which port it will exit. Then when one arm is much longer than the other, a photon which traverses the short arm would have to wait until the long arm has been traversed before exiting one way or the other.

Problems like these are removed when photons possess guidewaves to travel ahead and assess the instrument dimensions. Guidewaves interact with the beamsplitter and mirrors to determine the required division of amplitude, which governs the photon selection process.

Remarkable evidence for an advance guidewave field comes from an experiment by Brendel, Mohler & Martienssen (1991). Photon pairs produced by spontaneous parametric down-conversion were passed through a Michelson interferometer and detected by a time-resolved coincidence-detector. High visibility two-photon interference fringes were observed, even though the two photons must have travelled together down only one arm of the interferometer.

It should be possible to gain photon *which-way* information plus interference by sending the *idler* photon straight into one detector, prior to the *signal* photon entering the interferometer. Then the signal photon would take longer to traverse the long arm than the short arm, and reveal photon path selection. Confirmation of photon self-interference has been provided by Aspect & Grainger (1990) using a two beam Mach-Zehnder interferometer with a genuine one-photon source plus gated coincidence detection.

One way to confirm that a photon must interfere with its own guidewave is to replace a plane mirror of the interferometer by a cube corner reflector. This will reflect a bright coherent beam, but individual photons are displaced laterally so they cannot travel back along the same path to interfere.

3.3 Wiener's experiment

In this experiment, a photographic film is placed at a small angle to a mirror surface, see Jenkins & White (1957) p.217. Monochromatic light is then allowed to pass through the film and reflect from the mirror at normal incidence. In perfect agreement

with wave theory, the film is exposed by the light only where the electric field antinodes lie in the film.

Quantum theory would require that no photon is allowed to expose the photographic film directly from the top, but must first pass through the film to assess the mirror position before exposing the film in a fringe on its return journey. This constraint on photon interaction with the film does not arise when advance guidewaves can gauge the film-mirror spacing well before the photon reaches the film.

4 Entanglement

Many papers on the experimental confirmation of entanglement or non-local action have been published, see for example, Freedman & Clauser (1972), Aspect, Dalibard & Roger (1982), Chiao, Kwiat & Steinberg (1993), Rarity et al (1990), Ou et al (1990), Zbinden H et al (2001), Salart D et al (2008), and references therein.

Given the above description for guidewaves producing the observed interference phenomena, it is a small step to postulate that entanglement occurs when guidewaves from two photons interlink through each other coherently. A pair then results such that any external influence affecting one particle would be communicated rapidly to the other, as if the two particles constitute a single entity. A convenient time for entanglement to occur in photons would be during pair creation in down-converter crystals, as demonstrated in the references. Alternatively, stimulated emission of a photon in a laser would appear to involve coherent *guidewave* interaction from the stimulating photon rather than a direct photon-photon collision, see Blake & Scarl (1979). In the case of electrons in a superconductor, the periodic atomic structure at low temperature may help electrons coordinate into Cooper-pairs, via their coherent guidewaves. These examples indicate that physical guidewaves exist continuously between the components.

Derivation of a particle's de Broglie wavelength in Paper I assumed that the guidewaves propagate at the velocity of light, like electromagnetic field quanta. However they need not be arbitrarily restricted to the velocity of light, since relativity theory applies to a particle or photon as a whole, rather than their internal processes. In fact, we cannot rule out the possibility that entangled photons and particles could naturally communicate at superluminal velocity through their linking guidewaves. Evidence from experiments to investigate Bell's inequality may be interpreted here such that when one photon of a pair is detected, the entanglement breaks and the guidewave material flies

back to the other photon at superluminal velocity to carry back information regarding polarisation or spin. During flyback, the guidewave would be out of equilibrium so its velocity could be higher than normal, while it searches for new equilibrium. Dirac's equation appears to specify the velocity of light for the wavefunction, but it is only necessary for ($\hbar c$) to be constant; see Paper 1, Section 3.2. Schrödinger's non-relativistic equation is incomplete, and has no indication of the interaction velocity.

The experiment by Chiao, Kwiat & Steinberg (1993), following Franson, involved a down-converter crystal source of the entangled photons which went through identical Michelson interferometers, each with a long and short arm. Detected photons showed a degree of coincidence as if they had *pre-arranged* to both use either the long arm or short arm of their interferometers. To explain this in terms of guidewave theory, the two photons were continuously interlinked through their superluminal (≈ 4c) guidewaves *during* their travels from the source, and each photon sensed *both allowed paths* ahead. At the detectors, the two guidewaves decoupled and were gathered superluminally by their photons, ending all communication between the photons as they were absorbed by detector electrons.

An experiment on the timing of photon twins through a barrier versus free propagation also requires the two photons to sense both paths from start to finish. This compares with Young's double-slit experiment, wherein each photon has to sense the paths through both slits in order to interfere with itself at the screen.

5. The reality of trajectories, field quanta and particles

In standard quantum theory we are encouraged to disregard the reality of particle and quanta trajectories. Yet, by including these it is easier to comprehend how a fixed charge experiences force from a moving charge *as if* instantaneously; see French (1968) p.242.

Consider Figure 9, in which a moving charge q_1 at A emits a field quantum towards a stationary charge q_2 at P.

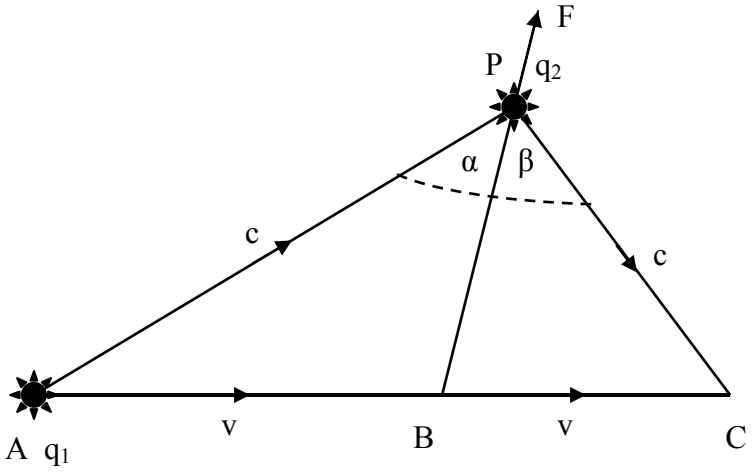

Fig. 9 Diagram showing the scattering of a field quantum emitted from q_1 at A, by a charge q_2 at P, such that it rejoins q_1 later at C.

It exerts a force on q_2 then returns to q_1 at C, thereby conserving total energy of q_1. If the velocity of q_1 is v and the quantum has the velocity of light c, then:

$$AB / AP = BC / PC = v/c . \qquad (5.1)$$

Geometry reveals that angles α and β are equal, so the quantum exerts a Newtonian force on q_2 , and the force vector F extrapolates back to the instantaneous position of q_1 at B even though the quantum was emitted from earlier position A. The interaction described is to be understood as an average over many field quanta. Some mystery remains in the way that the position of C is fixed in advance, as if superluminal guidewaves go ahead of the field quanta and charge q_1 to plan their trajectories.

6. Application to superconductivity

When the theory of electro-cordic field is applied to superconductivity, it accounts for electronic pairing primarily, followed by induced phonon resonance as a positive feedback interaction. Elsewhere there have been reviews of superconductivity in which pairing can be predominantly electronic while phonons are no longer central to the process, see for example Monthoux, Pines & Lonzarich (2007), Hackl & Hanke (2010), Oh et al, (2011), Dal Conte (2012). Various explanations for high temperature superconductivity are discussed in the book by Schrieffer & Brooks (2007). Here, a pairing mechanism will be introduced, which involves real material linking of electrons (the glue), rather than the tenuous assembling of coherent electrons in spite of Coulombic

repulsion in BCS theory. However, the acknowledged success of BCS theory for conventional superconductors does not appear to depend critically on the attractive mechanism between electrons. Consequently, a physically strong form of electron pairing and coherent assembly will now be described, while the BCS theory of energy gap, Meissner effect, etc., still operate as normal. Other criteria like doping, carrier concentration, specific heat, should also apply as in the literature.

Herein it is the real electronic guidewaves, as described by a mathematical wavefunction, which make electron pairing and correlation happen in all types of superconductors. Guidewaves emitted naturally by electrons induce two electrons to link together materially and form a circular loop structure, analogous to the electron spin-loop design (Wayte 2010). These electron-pairs only form around attractive positive lattice ions which screen the Coulomb repulsion, and can then be jostled free to wander through the lattice. The circumference of the loop is predicted to be equal to an electron de Broglie wavelength of (2x137) Compton wavelengths,

$$\lambda_B = 2 \times 137 \times \left(\frac{h}{mc} \right) = 6.650 \text{Å} \quad ; \qquad (6.1)$$

so the 2 electrons travel around the loop at velocity (c/274), with orbital angular momentum $2\hbar$ (for high temperature superconductors), see Figure 10.

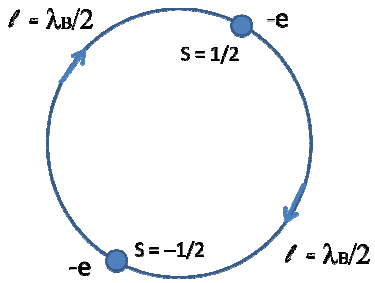

Figure 10 Electron-pair design for high temperature superconductors

However, for suitably-spaced lattice ions (~$\lambda_B/2$), neighbouring electron-pairs can immediately link materially under their own guidewave influence and form into a coherent cordeliere of parameter λ_B, with electron spins correlated to alternate anti-parallel, see Figure 11.

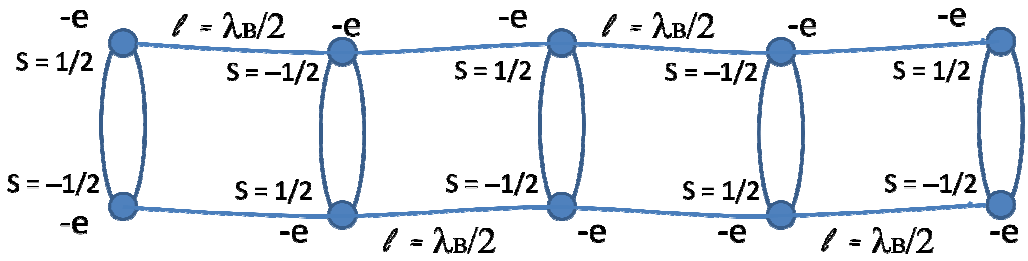

Figure 11 Electron-cordeliere design

This electron-cordeliere snakes through the crystal lattice, elastically without resistance, by stimulating resonance in these strings of ions which are influenced collectively by its Coulombic field (at frequency (c_s /λ_B), where c_s is sound velocity). Many adjacent cordelieres can become materially linked into an electron-quasiparticle, which stimulates a sheet of ions and consequently benefits from coherent positive feedback from phonons, rather than suffering from random thermal vibrations. This is where the BCS theory of phonon involvement may be justifiably applied, given that electron wavefunctions and de Broglie waves *really exist to implement* the multiple electron-pair phase coherence. When subjected to diagnostic techniques, quasiparticle structure will probably appear as current loops more than an electron-phonon interaction. The isotope effect should be compatible with this in general, although in high temperature superconductors it depends on doping and can be relatively small.

An energy analysis for electron-pair production is proposed as follows. Given that there is zero latent heat of transformation when forming a pair, then we need the Coulomb repulsion to be counteracted by an inherent electron-electron binding force akin to that holding the electron spin-loop together. Here, this has the form of a short-range nuclear force (Perkins, 2000) in one-dimension, where each electron emits some of its core material (the glue) to bind its partner electron. By considering this electron-pair as a single (non-radiating) particle, then the Coulomb repulsion acts around the circumference, as does the attractive force, see Figure 10. Total circumferential interaction force is to be:

$$F = \frac{e^2}{\varepsilon \ell^2} - \frac{e^2}{\varepsilon(\lambda_B/2)^2} \exp\left(1 - \frac{\ell}{(\lambda_B/2)}\right) , \qquad (6.2)$$

where ε is the local dielectric constant and ℓ is the circumferential distance between electrons. At equilibrium $(\ell = \lambda_B/2)$, there is no net force, see Figure 12.

Integration of Eq.(6.2) yields the work expended in forming the pair:

$$W = -\int_{\infty}^{\ell} F d\ell = \frac{e^2}{\varepsilon \ell} - \frac{e^2}{\varepsilon(\lambda_B / 2)} \exp\left(1 - \frac{\ell}{(\lambda_B / 2)}\right) . \qquad (6.3)$$

At final equilibrium $(\ell = \lambda_B / 2)$, zero work has been done overall; therefore the inherent kinetic energy of electron orbit velocity (c/274) must come from part of the total pair energy ($2mc^2$). In addition, no work has been done by the lattice ion which enables the process, so the pair is not bound to it. Figure 12 shows how work must be done against the Coulomb repulsion, from $\ell = \infty$ until the attractive force takes control at a critical distance $[\ell_c \approx 3.51(\lambda_B / 2)]$. In vacuo (ε = 1) this would require 880meV, but due to the positive central ion and surrounding dielectric constant in perovskites (i.e. screening) this may be reduced to a few meV, (Peter, Weger, Pitaevskii, 1998).

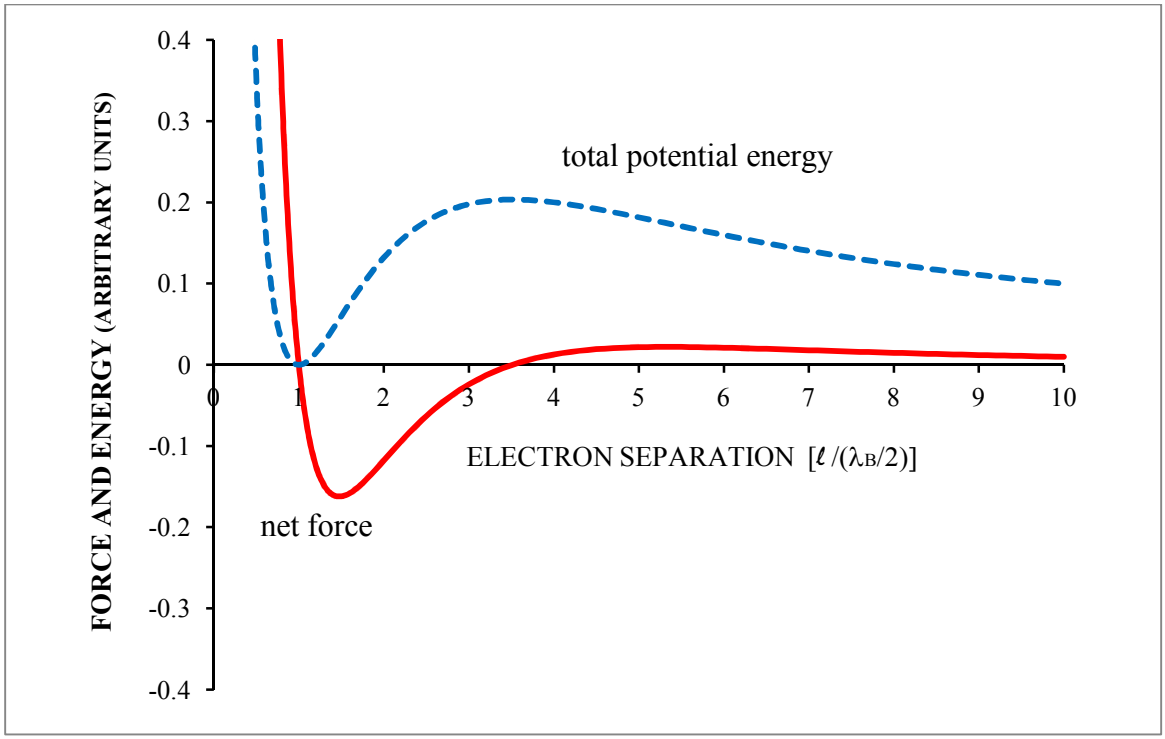

Figure 12 Net electron-electron force from Eq.(6.2) and total potential energy from Eq.(6.3). Electron separation distance around circumference is in units of $[\ell / (\lambda_B / 2)]$.

Now in order to stop the electron-cordelieres from being disrupted as easily as they are created, it is necessary for them to move from the high-ε charge reservoirs to the low-ε conduction region of the CuO_2 planes, where much greater thermal jostling will be

required to separate the electrons by their escape distance (ℓ_c). *It is this distinct layering of materials with different dielectric constants which preserves the electron-cordelieres and makes the high temperature superconductors superior.*

Given the above description of electron-pair creation with angular momentum $2\hbar$ for high temperature superconductors, it is equally applicable to the production of an electron-pair with zero angular momentum for conventional superconductors, wherein the electrons vibrate linearly at $\lambda_B/2$ separation. Even angular momentum $\hbar$ appears feasible for parallel electron spins.

In *all* superconductors, the above proposed ionic resonance mechanism depends on the structural parameters in an essential way for electron-cordeliere creation, and survival during conduction. For example, in orthorhombic YBCO we have [a = 3.823Å, b = 3.887Å, c = 11.680Å = 3.373Å (YCuO unit-cell) + 4.1535Å (BaCuO-cell) + 4.1535Å (BaCuO-cell)], according to Jorgensen et al (1990); therefore, the yttrium cell will resonate for (3.373Å x 2 ≈ λ_B). A perfect fit to λ_B is not necessary because guidewaves reflected from these Cu ions will still be almost in phase with the source electron-pair and its attached coherent pairs, in order to enhance resonance. Distance [2(Ba-Cu) ≈ λ_B] allows Cu ions to reflect guidewaves back constructively to the Ba layer where electron-pairs are created. The diagonal (Ba-Cu-Y ≈ λ_B) also partakes in the resonance, and assists the electron-cordeliere flowing through the lattice; probably zigzagging across the CuO_2 plane. For some iron-based superconductors, the anion height above the iron layer appears important; see Okabe et al (2010). This can be explained in terms of the distance [2x(La-As) ≈ λ_B] in LaFeAsO:F; or the distance [2x(Ba-As) ≈ λ_B] in $BaFe_2As_2$. The electron-pairs and cordelieres are produced in the LaO layer, but the superconducting flow is thought to be in the FeAs plane, supported by guidewave resonance.

In the following examples, the de Broglie wavelength is matched to lattice dimensions within a few percent, which assists electron-pair and cordeliere formation, and superconduction.

Tables 1a,b give the lattice parameters of several high temperature superconductors which are matched to resonance. Survival of coherence depends upon there being sufficient *in-phase reflections* from the surrounding ions, to enhance the extended guidewave links in spite of any jostling by the ions. Of course, other materials may satisfy this λ_B condition but fail to superconduct for different reasons; e.g. tetragonal

$YBa_2Cu_3O_{7-\delta}$. The Hg cuprates are interesting in that Hg-1223 has the highest T_c with its 3 CuO_2 layers, yet more layers are detrimental to T_c. One explanation for this is that the diagonal resonance (Ba- Cu- Ca $\approx \lambda_B$) is weakened by adding extra CuO_2 layers which allow leakage of the guidewaves and quasiparticles. Applied pressure up to 30GPa increases T_c by 25K according to Chu et al (1993) and Gao et al (1994). In fact for most cuprates, pressure causes a better fit to λ_B by a few percent, but this may not account totally for the increases in T_c . It is noteworthy that $CuBa_2Ca_3Cu_4O_{11-\delta}$ has the same T_c as Hg-1234 (see Liu et al. 1996), which shows that electron-pairing is not an aspect of the HgO/CuO charge reservoir layer.

Table 1a. Lattice parameters of some Cu-superconductors matched for resonance.

Superconductors	a, b (Å)	c (Å)	Resonance	Reference
$YBa_2Cu_3O_7$ Y-123 (92K)	a=3.8227 b=3.8872	11.68	2 x(Ba-Cu) $\approx \lambda_B$ Ba-Cu- Y $\approx \lambda_B$ 2 x Δc(Y) $\approx \lambda_B$	Jorgensen et al 1990
$HgBa_2CuO_4$ Hg-1201 (94K)	3.874	9.504	2 x(Ba-Cu) $\approx \lambda_B$ Ba-Cu-Ba $\approx \lambda_B$	Bertinotti et al 1996
$HgBa_2CaCu_2O_6$ Hg-1212 (128K)	3.855	12.665	2 x(Ba-Cu) $\approx \lambda_B$ Ba- Cu- Ca $\approx \lambda_B$	Radaelli et al 1993
$HgBa_2Ca_2Cu_3O_8$ Hg-1223 (134K)	3.851	15.830	2 x(Ba-Cu) $\approx \lambda_B$ Ba- Cu- Ca $\approx \lambda_B$	Bertinotti et al 1995
$HgBa_2Ca_3Cu_4O_{10}$ Hg-1234 (116K)	3.850	18.934	2 x(Ba-Cu) $\approx \lambda_B$ Ba- Cu- Ca $\approx \lambda_B$	Loureiro et al 1996
$HgBa_2Ca_4Cu_5O_{12}$ Hg-1245 (110K)	3.850	22.126	2 x(Ba-Cu) $\approx \lambda_B$ Ba- Cu- Ca $\approx \lambda_B$	Akimoto et al 1997
$CuBa_2Ca_3Cu_4O_{11}$ Cu-1234 (116K)	3.859	18.000	2 x(Ba-Cu) $\approx \lambda_B$ Ba- Cu- Ca $\approx \lambda_B$	Liu et al 1996
$Tl_2Ba_2CuO_6$ Tl-2201 (80K)	3.866	23.239	2 x(Ba-Cu) $\approx \lambda_B$ Ba-Cu-Ba $\approx \lambda_B$	Torardi et al 1988
$Tl_2Ba_2CaCu_2O_8$ Tl-2212 (108K)	3.855	29.318	2 x(Ba-Cu) $\approx \lambda_B$ Ba- Cu- Ca $\approx \lambda_B$	Subramanian et al 1988

$Tl_2Ba_2Ca_2Cu_3O_{10}$ Tl-2223 (125K)	3.853	35.640	2 x(Ba-Cu) ≈ λ_B Ba- Cu- Ca ≈ λ_B	Hasegawa,Matsushita, Takei 1996
$Bi_2Sr_2Ca_2Cu_3O_{10}$ Bi-2223 (110K)	a' = 5.411 b' = 5.409	37.082	2 x (Sr-Ca) ≈ λ_B Sr- Cu- Ca ≈ λ_B	Shamray,Mikhailova, Mitin (2009)

Table 1b. Lattice parameters of some Fe-superconductors matched for resonance.
Terms like Fe(1)-La(2) indicate a distance from one cell to the next.
Li(2)(±) is the averaged distance to both Li ions in the next cell.

Superconductors	a, b (Å)	c (Å)	Resonance	Reference
LaFeAsO:F 1111 (26K)	4.0195	8.6653	2 x(La- As) ≈ λ_B Fe(1)-La(2) ≈ λ_B	Nomura et al (2008)
CeFeAsO:F 1111 (41K)	3.9959	8.6522	2 x(Ce- As) ≈ λ_B Fe(1)-Ce(2)≈ λ_B	Zhao et al (2008)
SmFeAsO:F 1111 (43K)	a'=5.5611 b'=5.5732	8.4714	2 x(Sm-As) ≈ λ_B Fe(1)-Sm(2)≈λ_B	Martinelli et al (2008)
NdFeAsO 1111 (51K)	3.9467	8.531	2 x(Nd-As) ≈ λ_B Fe(1)-Nd(2)≈ λ_B	Kumai et al (2009)
$BaFe_2As_2$ 122 (29K)	3.9570	12.968	2 x(Ba-As) ≈ λ_B Fe(1)-Ba(2)≈ λ_B	Alireza et al (2009)
$SrFe_2As_2$ 122 (27K)	3.917	12.36	2 x(Sr-As) ≈ λ_B Fe(1)-Sr(2) ≈ λ_B	Zhao et al (2008) Schnelle et al (2009)
LiFeAs 111 (16K)	3.775	6.355	Fe(1)-Li(2)(±) ≈ λ_B	Pitcher et al (2008)
NaFeAs 111 (9-30K)	3.9473	6.9911	2 x(Fe-Na) ≈ λ_B 2 x(Na-Na)≈ λ_B	Parker et al (2008) Liu et al (2011)
FeSe 11 (8K)	3.769	5.4861	Fe-Fe ≈ λ_B (diagonal)	Hsu et al (2008) Margadonna et al

Table 2 covers compound superconductors, where we have for example hexagonal MgB_2 with [a = 3.0823Å, c = 3.5146Å] according to Jorgensen et al (2001); therefore the unit plane of Mg will resonate for guidewave reflections from neighbouring ions, ie: the average of 2*a* and 2*c* is around λ_B. Some stretching of a cable sample by 1% would match λ_B better and probably increase T_c by 2K, see Tang et al (2001).

Table 2. Lattice parameters of some compound superconductors matched for resonance.

Superconductor	a (Å)	c (Å)	Resonance	Reference
MgB_2 (39K)	3.0822	3.5146	$a + c \approx \lambda_B$ averaged	Jorgensen et al 2001
Nb_3Sn (18.3K)	5.29	5.29	2 x(Nb-Nb) $\approx \lambda_B$	Escudero, Morales 2010
Nb_3Ge (23.6)	5.17	5.17	2 x(Nb-Nb) $\approx \lambda_B$	Paduani 2007
Nb_3Ga (20.2)	5.17	5.17	2 x(Nb-Nb) $\approx \lambda_B$	Paduani 2007
Nb_3Al (18.8)	5.19	5.19	2 x(Nb-Nb) $\approx \lambda_B$	Paduani 2007
NbN (16K)	4.39	4.39	2 x(Nb-Nb) $\approx \lambda_B$ (diagonal)	Shiino et al 2009
ZrN (10K)	4.59	4.59	2 x(Zr-Zr) $\approx \lambda_B$ (diagonal)	Saha et al 2010
TiN (5.6K)	4.22	4.22	2 x(Ti-Ti) $\approx \lambda_B$ (diagonal)	LeClair, Berera, Moodera 2000
Rb_3C_{60} (29.5K)	14.38	14.38	2x(Rb-Rb) $\approx 3\lambda_B$ (diagonal)	Saito et al 2004

Table 3 shows how many elemental Type I superconductors are matched to resonance. Elements Na, K, Rb, Mn, Co, Cu, Ag, Au, may not be superconductors because they are inefficient at electron-pair creation and lattice resonance feedback.

Table 3. Lattice parameters of some Type I superconductors matched for resonance.
Notation (a,b,c) etc. indicates distance from origin, ie. $(a^2+b^2+c^2)^{1/2}$.
Reference: www.superconductors.org/Type1.htm

Superconductor		a, b (Å)	c (Å)	Resonance	Type
Pb	(7.196K)	4.9508	4.9508	$2(a/2,0,c/2) \approx \lambda_B$	FCC
La	(4.88K)	3.772	12.144	$(a,b,0) \approx \lambda_B$	HEX
Ta	(4.47K)	3.3013	3.3013	$2a \approx \lambda_B$	BCC
Hg	(4.15K)	3.005	3.005	$2(-a,0,c) \approx \lambda_B$	RHL
Sn	(3.72K)	5.8318	3.1819	$2c \approx \lambda_B$	TET
In	(3.41K)	3.2523	4.9461	$2a \approx \lambda_B$	TET
Tl	(2.38K)	3.4566	5.5248	$2a \approx \lambda_B$	HEX
Re	(1.697K)	2.761	4.456	$(a,b,c) \approx \lambda_B$	HEX
Pa	(1.40K)	3.925	3.238	$2c \approx \lambda_B$	TET
Th	(1.38K)	5.0842	5.0842	$2(a/2,b/2,0) \approx \lambda_B$	FCC
Al	(1.175K)	4.0495	4.0495	$(a,b,c) \approx \lambda_B$	FCC
Ga	(1.083K)	4.52	7.6633	$(a,b,0) \approx \lambda_B$	ORC
Mo	(0.915K)	3.147	3.147	$2a \approx \lambda_B$	BCC
Zn	(0.85K)	2.669	4.9468	$(a,b,c) \approx \lambda_B$	HEX

To get higher T_c in the future, the CuO_2 planes in cuprates might be compounded/mixed/interleaved under high temperature/pressure with material of lower dielectric constant, while retaining the lattice parameters supporting guidewave resonance; for example, add oxides of Sn, Zn, Ni, and various dopants. The iron-pnictide superconductors can be improved in a corresponding manner. Besides sintering bulk mixtures, one could sputter and laminate materials onto different cores, or try diffusion and implantation. A sample of coaxial cable containing superconducting surface layers could have a travelling electric field applied to encourage electron flow over the surface, where ε is lower. Evacuation might also help.

8. Conclusion

The physical nature of proposed electro-cordic guidewaves has been demonstrated by applying guidewave theory to relativistic potential wells and simple harmonic motion, interference phenomena, entanglement and superconductivity. The guidewave quanta described mathematically by the wavefunction travel ahead of particles and photons, and link entangled pairs. Overall, the interpretation of quantum theory can be self-consistent and physically reasonable by making it more causal; and this will allow continuity into the realms of particle and photon *structure*.

Acknowledgements

I would like to thank Imperial College Libraries and A. Rutledge for typing.

References

Akimoto J, et al, (1997)

Alireza P, et al, (2009) J Phys, Con Matt 21, 012208

Aspect A, Dalibard J & Roger G, (1982) Phys Rev Lett 49, 1804

Aspect A & Grainger P, (1990) Sixty two years of uncertainty. Ed A I Miller, Plenum Press, N York, p 45

Bertinotti A, et al, (1995) Physica C 250, 213

Bertinotti A, et al, (1996) Physica C 268, 257

Blake G D & Scarl D, (1979) Phys Rev A 19, 1948

Bohm D & Hiley B J, (1993) The Undivided Universe, Routledge, London

Brendel J, Mohler E & Martienssen W, (1991) Phys Rev Lett 66, 1142

Chiao R Y, Kwiat P G & Steinberg A M, (1993) Sci Amer, August, 38

Chu CW, et al, (1993) Nature 365, 323

Dal Conte S, et al, (2012) Science 335, 1600

Durr S, Nonn T & Rempe G, (1998) Phys Rev Lett 81, 5705

Escudero R & Morales F, (2010) Sol State Comm 150, 715

Fonseca E J S, et al, (1999) Phys Rev A 60, 1530

Freedman S J & Clauser J F, (1972) Phys Rev Lett 28, 938

French A P, (1968) Special Relativity, Nelson, UK

Gao, et al, (1994) Phys Rev B50, 4260

Glazier E V D & Lamont H R L, (1958) The Services Textbook of Radio, Vol 5 Transmission and Propagation, HMSO London

Hasegawa M, Matsushita Y & Takei H, (1996) Physica C 267, 31

Hitachi, (2008) www.hitachi.com/rd/research/em/doubleslit.html

Hackl R & Hanke W, (2010) Eur Phys J Special Topics 188, 3

Hsu FC, et al, (2008) Proc Nat Acad Sci USA 105, 14262

Jenkins F A & White H E, (1957) Fundamentals of Optics, McGraw Hill, N York

Jönsson C, (1974) American J Phys 42, 4

Jorgensen J D, et al, (1990) Phys Rev B 41, 1863

Jorgensen J D, et al, (2001) Phys Rev B 63, 224522

Kumai R, et al, (2009) J Phys Soc Jap 78, 013705

LeClair P, Berera G P & Moodera J S, (2000) Thin Solid Films 376, 9

Liu Q, et al, (2011) J. Am. Chem. Soc 133 (20), 7892

Liu C J, et al, (1996) Phys Rev B 53, 5170

Loureiro S M, et al, (1996) Physica C 257, 117

Shamray V F, Mikhailova A B & Mitin A V, (2009) Crystallography Reports 54, 584

Margadonna S, et al, (2008) arXiv:0807.4610

Martinelli A, et al, (2008) arXiv:0808.1024

Monthoux P, Pines D & Lonzarich G G, (2007) Nature 450, 1177

Nomura T, et al, (2008) J Phys Soc Jpn 77, Suppl C p32

Oh H, et al, (2011) Progress in superconductivity 13, 65

Okabe H, et al, (2010) Phys Rev B 81, 205119

Ou Z Y, et al, (1990) Phys Rev A 42, 2957

Paduani C, (2007) Brazilian J Phys 37, 1073

Parker D, et al, (2008) arXiv:0810.3214

Perkins D H, (2000) *Introduction to High Energy Physics, 4th Ed*, CUP, Cambridge

Peter M, Weger M & Pitaevskii LP, (1998) Ann Physik 7, 174

Pfleegor R L & Mandel L, (1967) Phys Rev 159, 1084

Pitcher M, et al, (2008) arXiv:0807.2228

Radaelli P G, et al, (1993) Physica C 216, 29

Rarity J G, et al, (1990) Phys Rev Lett 65, 1348

Saha B, et al, (2010) J App Phys 107, 033715

Saito S, et al, (2004) Sol State Comm 130, 335

Salart D, et al, (2008) Nature 454, 861

Schiff L I, (1968) Quantum Mechanics 3rd edition, McGraw-Hill, N York

Schrieffer J R & Brooks J S, (2007) Handbook of high-temperature superconductivity, Springer, NY.

Selleri F, (1982) Found Phys 12, 1087

Schnell W, et al, (2009) Physical Review B 79, 214516

Subramanian M A, et al, (1988) Nature 332, 420

Tang J, et al, (2001) Phys Rev B 64, 132509

Terman F E, (1955) Electronic and Radio Engineering 4th edition, McGraw-Hill, N York

Torardi C C, et al, (1988) Phys Rev B 38, 225

Wayte R, (2012) www.vixra.org/abs/1208.0208 ''Theory of an electro-cordic field operating in quantum systems I''

Wayte R, (2010) www.vixra.org/abs/1007.0055 ''A Model of the Electron''

Zbinden H, et al, (2001) J Phys A: Math Gen 34, 7103

Zhao J, et al, (2008) Phys Rev B 78, 140504(R)

Zhao J, et al, (2008) Nat Mat 7, 953